optica

Monolithic frequency comb platform based on interband cascade lasers and detectors

Benedikt Schwarz,[1,*] Johannes Hillbrand,[1] Maximilian Beiser,[1] Aaron Maxwell Andrews,[1] Gottfried Strasser,[1,2] Hermann Detz,[2,3] Anne Schade,[4] Robert Weih,[5] and Sven Höfling[4,6]

[1]Institute of Solid State Electronics, TU Wien, Vienna, Austria
[2]Center for Micro- and Nanostructures, TU Wien, Vienna, Austria
[3]Central European Institute of Technology, Brno University of Technology, Brno, Czech Republic
[4]Technische Physik, Physikalisches Institut, University Würzburg, Am Hubland, 97074 Würzburg, Germany
[5]Nanoplus Nanosystems and Technologies GmbH, 97218 Gerbrunn, Germany
[6]SUPA, School of Physics and Astronomy, University of St Andrews, St Andrews, KY16 9SS, UK
*Corresponding author: benedikt.schwarz@tuwien.ac.at

Received 26 April 2019; revised 8 June 2019; accepted 11 June 2019 (Doc. ID 366112); published 12 July 2019

New insights into the laser dynamics of interband cascade lasers reveal the possibility to generate frequency-modulated combs by utilizing their inherent gain nonlinearity. The resulting comb state is characterized by chirped instantaneous frequency, which appears to be universal to frequency combs based on gain-induced four-wave mixing. The fast dynamics in the injectors further allow the realization of exceptionally sensitive and high-speed photodetectors, operating at room temperature, using the very same epilayer structure. With the capability of integrating frequency combs and ultra-fast detectors on a single chip consuming less than a watt of electric power, interband cascade laser technology provides a complete and unmatched platform for future monolithic and battery-driven dual-comb spectrometers.

https://doi.org/10.1364/OPTICA.6.000890

1. INTRODUCTION

Sensors are the heart of every smart technology. They allow us to capture data about environmental pollution, plant infections, or our current physiological condition. The mid-infrared region is the spectral region of choice when it comes to sensing and spectroscopy. No other spectral region provides the same sensitivity or selectivity for molecular fingerprinting. Established mid-infrared spectrometers are mostly based on free-space optics and moving parts. None of these concepts can be sufficiently down-scaled to single-chip dimensions. Dual-comb spectroscopy [1–4] offers the possibility to directly map the optical spectrum to the radio-frequency (RF) domain. Dual-comb spectrometers do not require movable parts and can be miniaturized without losing spectral resolution—there is no relation between the spectral resolution and the spatial dimension. Its full potential for practical applications can be unlocked if both frequency comb generators and heterodyne detectors are miniaturized, driven by a battery and ideally integrated on a single chip.

For a long time, frequency comb generation in the mid-infrared was limited to table-top instruments [5,6]. Relatively compact setups can be realized using near-infrared frequency combs combined with difference frequency generation [7,8]. Even more potential for integration was demonstrated utilizing the Kerr nonlinearity in passive microresonators [9,10]. While microresonator combs recently reached the maturity to enable compact and battery-driven systems at telecom wavelengths [11], frequency comb generation in the mid-infrared is still restricted to external pump lasers. An alternative concept employs the nonlinearity of the laser itself. This per se monolithic approach is ideal for the realization of miniaturized spectrometers and was found in quantum cascade lasers (QCLs) a few years ago [12]. Recently, passive mode-locking was achieved using GaSb-based type I cascade diode lasers [13]. With this, mode-locked semiconductor diode lasers are starting to be available in the range of 2–3.5 μm.

An ideal low-power alternative operating also at longer wavelength up to 6 μm is constituted by interband cascade lasers (ICLs) [14–16]. Their power consumption is 1–2 orders of magnitude smaller than that of QCLs. Also, in terms of output power and efficiency, ICLs are catching up rapidly [15,17,18,19]. Their potential for multi-heterodyne spectroscopy was already highlighted using multi-mode Fabry–Perot ICLs and computational correction algorithms to acquire 16 lines in parallel [20]. Robust low-phase noise frequency comb operation, as demonstrated here, will enable dual-comb spectroscopy with the capability to simultaneously acquire more than a hundred modes.

In this work, we present a monolithic frequency comb sensing platform utilizing the fast dynamics in ICLs. These fast dynamics enable frequency-modulated comb operation as well as

the realization of ultra-fast photodetectors using the same ICL material and hence provide a monolithic platform for dual-comb spectroscopy. Our findings and conclusions on frequency comb operation are different from those of recent works that focused on comb generation via passive mode-locking of ICLs [21] and suggest that a careful reinterpretation of those results is required. (Recent results on passive mode-locking of ICLs [23] include both a second-order autocorrelation as well as a multi-heterodyne beat trace, which show no sign of pulse formation, lacking the 8:1 ratio in the autocorrelation and pulses in the multi-heterodyne beat trace.) The ICL frequency combs presented in this letter rely on the inherent gain nonlinearity caused by the fast-gain dynamics. They do not require a saturable absorber, and show they the same phase characteristics as QCL frequency combs.

2. FREQUENCY-MODULATED COMBS USING ICLS

In order to investigate frequency comb operation of ICLs, we fabricated a two-section device [Fig. 1(a)]. The short section is optimized for a low parasitic capacitance of the contacts for efficient radio-frequency (RF) extraction and injection. Its DC bias can be adjusted to alter the locking properties [24]. It is important to note that the DC bias remains in the forward direction and here is only used to fine-tune the group velocity dispersion or the spectral lineshape of the round-trip gain. This is fundamentally different to passive mode-locking, e.g., in quantum well lasers, where the short section is used to provide fast saturable loss using a strong reverse bias [13]. The high frequency-modulation response provides important information about the internal gain dynamics. The extracted frequency response is flat up to 20 GHz and reveals that the characteristic response time of the population inversion $\tau_{\Delta n}$ is fast enough such that population oscillations can occur at least at the first two harmonics of the repetition frequency. Since the condition $\tau_{\Delta n} f_{\mathrm{rep}} \lesssim 1$ is satisfied, four-wave mixing via population inversion oscillations can be assumed to be the dominant contribution to the gain nonlinearity [25] and enables self-starting frequency comb operation.

A first indication for frequency comb operation is the observation of a narrow beat note. In multi-mode lasers, each mode pair causes a beating at their difference frequency. In frequency combs all modes are equidistant, resulting in a narrow beat note. Hence, the observation of a narrow beat note is a first indication of frequency comb operation. This beat note can be observed using a fast photodetector (optical) or directly extracted from the laser driving current (electrical)—provided that the gain dynamics are fast enough to follow the beating. Figure 1(b) shows the

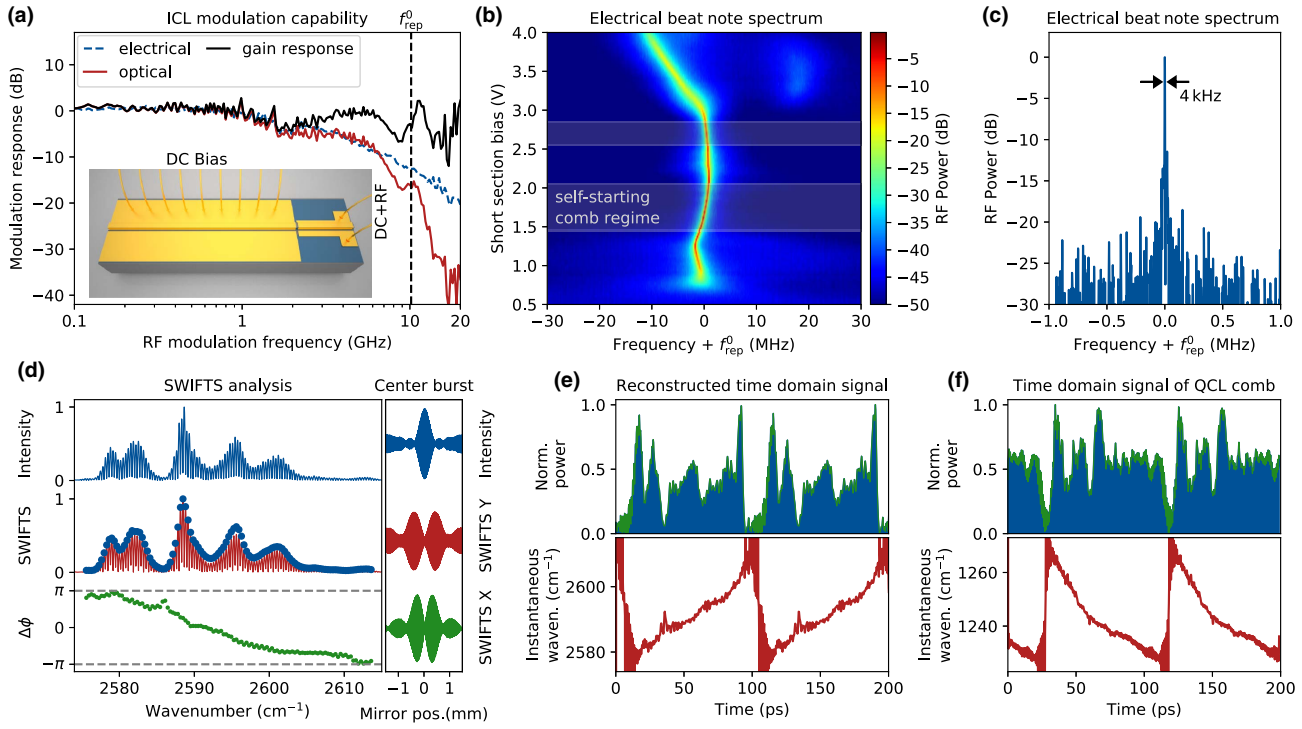

Fig. 1. ICL frequency comb. (a) Frequency-modulation capabilities of the optimized devices measured optically via a fast QWIP (red) and electrically via RF rectification [22] (blue). The black curve is corrected by the contribution due to the parasitic capacitance of the ICL and QWIP response to extract the portion due to the response of the gain medium. Inset: sketch of the two-section device. (b) The spectral lines of the ICL beat together, leading to a modulation of the laser intensity at the cavity round-trip frequency. The resulting electrical beat note can be measured by recording the RF spectrum of the absorber current and tunes with the absorber bias. Regions of self-starting comb operation are highlighted by the rectangles. (c) Narrow electrical beat note with a linewidth of 4 kHz. (d, e) Shifted Wave Intermode Beat Fourier Transform Spectroscopy (SWIFTS) analysis and corresponding time-domain signal of the ICL frequency comb. The intermode difference phases cover the range from π to $-\pi$. This and the minimum in the SWIFTS interferograms at zero-phase are characteristic for the suppression of amplitude modulation. The spectrum consists of 114 modes spaced by $f^0_{\mathrm{rep}} = 10.17$ GHz. The mode grouping might be due to parasitic reflections in the two-section laser. (f) Time-domain signal of a QCL frequency comb [23]. Irrespective of the sign, the both combs show the same characteristic dominantly frequency-modulated output. This suggests that the ICL frequency comb is indeed governed by the inherent gain nonlinearity, which is connected to the suppression of amplitude modulations.

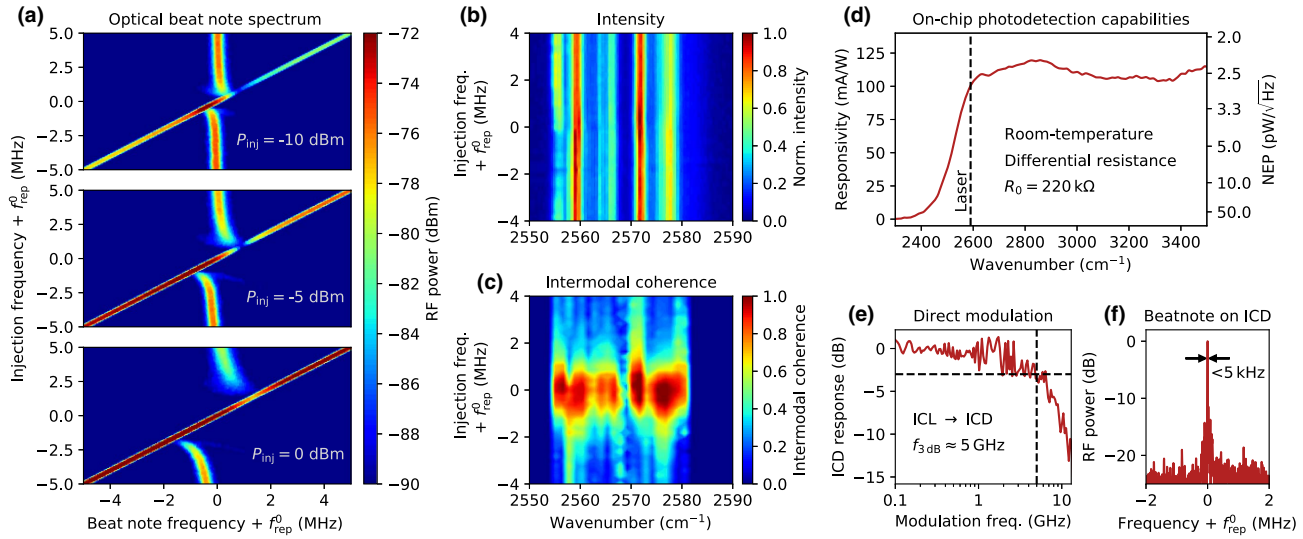

Fig. 2. Coherent injection-locking and on-chip detection capabilities. (a) Optical beat note spectrum of the ICL depending on the injection frequency for three different injection powers. The large locking range is due to the optimized RF injection. (b, c) Intensity and SWIFTS spectral maps at 5 dB injection power as a function of the injection frequency. (d) Spectral responsivity and noise equivalent power of the on-chip interband cascade detector (ICD), which was cleaved from the same chip. (e) Direct modulation response of the ICL measured with the ICD. (f) Narrow beat note of the ICL comb measured with the ICD. (f^0_{rep} = 10.17 GHz).

electrically extracted laser beat note depending on the short section bias. The latter can be altered to tune the ICL into the self-locking regime. There, the beat note appears narrow with a linewidth on the kilohertz (kHz) level [Fig. 1(c)].

In order to unequivocally prove frequency comb operation, we employ shifted wave intermode beat Fourier transform spectroscopy (SWIFTS) [26,27]. This technique provides a complete characterization of a comb state by measuring the coherence and phase between each pair of comb lines (for details, see the methods section). The SWIFTS analysis of the ICL frequency comb is plotted in Fig. 1(d). The amplitudes of the SWIFTS spectrum match the beating amplitudes extracted from the intensity spectrum (blue dots), which serves as a proof for comb operation over the entire emission spectrum. The minimum of the SWIFTS interferograms at zero path difference is a clear sign of the suppression of amplitude modulations. This phenomenon is known to be related to fast-gain dynamics [12]. Even more exciting is additional information provided by the phases. The intermodal phases follow a chirped pattern covering a range of 2π. The same pattern was recently observed in QCLs [28]. Figures 1(e) and 1(f) show the direct comparison of the time-domain signals of an ICL and a QCL frequency comb. Although the laser transition lifetimes differ by 2 orders of magnitude and operate at a different wavelength, both frequency combs show the linearly chirped instantaneous frequency accompanied by the suppression of amplitude modulations. This remarkable similarity indicates that the comb formation is indeed governed by the same physical mechanism—four-wave mixing due to population inversion oscillations. A state with small-amplitude modulation maximizes the round-trip gain, as amplitude modulations lead to a stronger gain saturation in fast-gain media. This is the opposite of passive mode-locking in slow-gain media with a fast saturable absorber, where the gain section is too slow to respond to intermode beatings. There, the formation of pulses is advantageous, as it minimizes the round-trip loss. Recent theoretical work revealed that phase-locking in frequency-modulated combs is governed by the combined effects of a Kerr nonlinearity due to a non-zero linewidth enhancement factor (asymmetric spectral gain profile) in fast-gain media and the group velocity dispersion [29]. The sign of these effects define the direction of the chirp, which might be due to an in-plane dispersion relation that leads to opposite signs of the linewidth enhancement factor in QCLs and ICLs.

Recent findings revealed that the repetition frequency of a QCL frequency comb can be injection-locked to an external RF oscillator while maintaining full intermodal coherence [23]. This enables all-electric stabilization similarly to phase-locked loops [30] and additionally increases the range of comb operation and the stability against optical feedback. This technique can also be employed with ICL frequency combs. Figure 2(a) shows the optically measured beat note spectrum while sweeping the injection frequency across the beat note for three different injection power levels. As the frequency of the injected signal approaches the beat note, the latter is pulled towards it. The laser beat note is fully controlled by the external RF oscillator within a locking range of 1, 2, and 4 MHz, depending on the power of the injected signal. Figures 2(b) and 2(c) show the intensity spectrum as well as the intermodal coherence spectrum depending on the injection frequency. The color map in Fig. 2(c) shows that full intermodal coherence and thus frequency comb operation is achieved within the locking range.

3. MONOLITHIC ULTRA-FAST DETECTORS USING ICLS

Integrating a complete dual-comb spectrometer on a chip requires a technology that is capable of both frequency comb operation and high-speed multi-heterodyne detection. This can be achieved by self-detection [31] or using on-chip integrated photodetectors. An elegant solution is building the laser and detector from the very same material. This so-called bi-functional operation was first demonstrated using QCLs [32] and trigged the realization

of a monolithic lab-on-a-chip [33]. However, the additional on-chip detection feature requires significant modifications of the QCL design to match the laser and detector wavelength. Hence, bi-functional QCLs were restricted to pulsed operation for a long time [34]. Fortunately the bi-functional operation of ICLs comes naturally and does not require modifications of the design [35]. The longer lifetime of the optical transition decreases the thermal noise and increases the internal quantum efficiency. Figure 2(d) shows the spectral responsivity of the interband cascade detector (ICD) that was fabricated on the same chip and cleaved for characterization. A broadband spectral responsivity of over 100 mA/W and an exceptionally low noise equivalent power of 2.5 pW$\sqrt{\text{Hz}}$ are achieved at room temperature. The provided, yet not optimized, ICD performance is clearly superior to bi-functional QCL material. In order to demonstrate the high-speed operation, which is essential for multi-heterodyne detection, we measured the ICD frequency response optically using the ICL [Fig. 2(e)]. The large detection bandwidth even enables the measurement of the beat note of the ICL frequency comb with an SNR of 22 dB at room temperature [Fig. 2(f)]. The high-frequency cutoff around 5 GHz includes both the laser and the detector response. While this significantly exceeds previous reports on a 800 MHz combined cutoff (1.3 GHz detector cutoff) [36], the high frequency response remains limited by the parasitic capacitances of the devices and suggests that the fundamental carrier transit time limit is still not reached. Even higher cutoffs of 26 GHz have been realized using quantum well infrared photodetectors (QWIPs) [37], as the typically much larger number of periods reduces the parasitic capacitance. These results highlight the remarkable detection capabilities provided by the ICL comb platform. Integrated on the same chip, the coupling efficiencies are much higher compared to free-space optics, and further, the size of the detector can be decreased to reduce the noise [33,34]. In principle, a monolithic sensor chip with a few centimeters of interaction length can thus achieve the same detector noise limited sensitivity as a setup with discrete elements and an interaction length of a few meters. We further want to highlight the major benefit of the dual-comb technique for integration with respect to electrical crosstalk, which was the main limiting factor in previous integrated laser/detector sensor chips operating in pulsed mode. The multi-heterodyne beat signal is commonly recorded at a very different frequency range (e.g., 10 MHz–1 GHz) [30] compared to the DC bias and the 10 GHz RF modulation of the lasers and hence should be free from electrical crosstalk.

4. CONCLUSION

We presented new insights into the dynamics of interband cascade lasers for frequency comb generation and highlighted their enormous potential for miniaturization. ICLs provide all the properties for future ultra-compact and battery-driven dual-comb sensors as summarized in Table 1. We demonstrated self-starting ICL frequency combs based on the inherent gain nonlinearity caused by the fast dynamics of the population inversion. The resulting frequency comb state shows a dominant frequency modulation and a linearly chirped phase signature, which is characteristic for the suppression of amplitude modulations in fast-gain media. ICL technology reduces the power consumption by 2 orders of magnitude compared to QCL to below 1 W, enabling battery-driven sensors. Furthermore, ICLs provide exceptionally sensitive and high-speed photodetection capabilities that allow monolithic integration of all active optical components. Thus, ICL technology provides all the properties for all-solid-state mid-infrared sensors and will promote dual-comb spectroscopy from fundamental research to a broadly used sensing platform.

Table 1. The Presented ICL Frequency Comb Platform is the Only Available Mid-Infrared Technology that Meets All Requirements to Build Ultra-Compact and Battery-Driven Dual-Comb Spectrometers

Requirements	Microresonator	QCL	ICL
Comb operation	∘	∘	•
Stabilization knobs	∘	∘	•
Compact	–[a]	∘	•
Battery-driven	–[a]	–	•
GHz on-chip detection	–	∘	•

(–) not demonstrated, (∘) demonstrated, (•) this work.
[a]Only in the near-infrared [11].

APPENDIX A. METHODS

A. DEVICE FABRICATION

The investigated ICLs were grown at the Universität Würzburg and at Nanoplus GmbH and processed at the Center of Micro- and Nanostructures at TU Wien. The simulated bandstructure is shown in Supplement 1, Fig. S6. The laser ridges (6 μm wide and 4 mm long) were fabricated with standard mask photolithography, reactive ion etching to define the laser waveguides, silicon nitride for the passivation layers, and sputtered TiAu for the contact pads. The substrate was thinned to 160 μm, and TiAu was sputtered on the backside. The devices were mounted epi-side-up using indium on a copper mount. Different thickness of the passivation layer have been used to optimize the device performance in terms of output power and modulation capability.

B. MEASUREMENT SETUP

The devices were mounted on a copper submount, thermoelectrically stabilized to 15°C. In order to improve the noise properties of our laser driver, we used home-built low-pass filters. The accuracy of temperature stabilization and the noise of the laser drivers play a crucial role for the stability of the frequency comb. The spectral response of the detector was measured using a thermal broadband source and a collimation lens. The detector was mounted on a motorized $x-y$ translation state to measure the spatial overlap of the facet with the focal spot to obtain the coupling efficiency. A calibrated power meter was used as a reference. The thermal noise limited noise equivalent power (NEP) was extracted using the measured responsivity and device resistance. A more detailed description can be found in Ref. [38].

C. RELEVANCE OF THE SPATIAL BEAT NOTE PROFILE

An important aspect that must be considered for injection-locking is the spatial patterns of the laser beat note in standing-wave lasers [39]. Because of the boundary condition of the modes in the cavity, all beatings between adjacent lines will follow a half-wave cosine function along the cavity. Hence, the modulation should be applied at the end of the cavity, where the laser is most susceptible to injection-locking.

APPENDIX B. SWIFTS

The SWIFTS concept was realized using a fast quantum well infrared photodetector (QWIP) placed at the output window of a Fourier transform infrared spectrometer (FTIR) (sketch in Supplement 1, Fig. S5). The emitted light of the ICL is shined through the FTIR onto the QWIP. A local oscillator mixes down the optical beat note of the ICL to ≈40 MHz. By recording the quadrature components X and Y of the QWIP signal in dependence of the delay time τ using a lock-in amplifier, we obtain the two SWIFTS quadrature interferograms. The reference signal for the lock-in amplifier is obtained by mixing another local oscillator with the RF source used for injection into the ICL. All interferograms were recorded by the lock-in using the He–Ne trigger of the FTIR. Our FTIR (Bruker Vertex 70v) moves each arm by $\pm\tau/2$. The complex sum of the interferograms is therefore given by

$$F(X+iY)(\tau)=\sum_n A_n A_{n-1}\left[\cos\left(\frac{\omega_r\tau}{2}\right)+\cos(\omega_{n-1/2}\tau)\right]. \quad \text{(B1)}$$

By applying a fast Fourier transformation using zero-padding and peak fitting, both amplitude and phase of all intermode beatings are obtained. The intermode beatings describe the coherence and phases between adjacent comb modes. The normalized intermodal coherence can be defined as [27]

$$c=\frac{|\langle A_n A_{n-1} e^{(i(\varphi_n-\varphi_{n-1}))}\rangle|}{\langle |A_n||A_{n-1}|\rangle}, \quad \text{(B2)}$$

where A_n are the field amplitudes, φ_n the intermodal phases, and the brackets denote temporal averaging. The phases of the modes can be calculated by the cumulative sum of the intermode beating phases, which together with the intensity spectrum allows the reconstruction of the time-domain signal of a comb state.

Funding. Austrian Science Fund (FWF) (F4909-N23, P28914-N27, W1243); European Social Fund (ESF) (CZ.02.2.69/0.0/0.0/16_027/0008371); Air Force Office of Scientific Research (AFOSR) (FA9550-17-1-0340); Österreichische Forschungsförderungsgesellschaft (FFG) (849614, 861581).

Acknowledgment. The authors thank A. Belyanin for the fruitful discussions at IQCLSW 2018. H. D. and A. M. A. were supported by the ESF project.

See Supplement 1 for supporting content.

REFERENCES

1. S. Schiller, "Spectrometry with frequency combs," Opt. Lett. **27**, 766–768 (2002).
2. F. Keilmann, C. Gohle, and R. Holzwarth, "Time-domain mid-infrared frequency-comb spectrometer," Opt. Lett. **29**, 1542–1544 (2004).
3. I. Coddington, N. Newbury, and W. Swann, "Dual-comb spectroscopy," Optica **3**, 414–426 (2016).
4. G. Ycas, F. R. Giorgetta, E. Baumann, I. Coddington, D. Herman, S. A. Diddams, and N. R. Newbury, "High-coherence mid-infrared dual-comb spectroscopy spanning 2.6 to 5.2 μm," Nat. Photonics **12**, 202–208 (2018).
5. D. T. Reid, B. J. S. Gale, and J. Sun, "Frequency comb generation and carrier-envelope phase control in femtosecond optical parametric oscillators," Laser Phys. **18**, 87–103 (2008).
6. G. Andriukaitis, T. Balčiūnas, S. Ališauskas, A. Pugžlys, A. Baltuška, T. Popmintchev, M.-C. Chen, M. M. Murnane, and H. C. Kapteyn, "90 GW peak power few-cycle mid-infrared pulses from an optical parametric amplifier," Opt. Lett. **36**, 2755–2757 (2011).
7. A. Schliesser, N. Picqué, and T. W. Hänsch, "Mid-infrared frequency combs," Nat. Photonics **6**, 440–449 (2012).
8. P. G. Schunemann, K. T. Zawilski, L. A. Pomeranz, D. J. Creeden, and P. A. Budni, "Advances in nonlinear optical crystals for mid-infrared coherent sources," J. Opt. Soc. Am. B **33**, D36–D43 (2016).
9. P. Del'Haye, A. Schliesser, O. Arcizet, T. Wilken, R. Holzwarth, and T. J. Kippenberg, "Optical frequency comb generation from a monolithic microresonator," Nature **450**, 1214–1217 (2007).
10. T. J. Kippenberg, R. Holzwarth, and S. A. Diddams, "Microresonator-based optical frequency combs," Science **332**, 555–559 (2011).
11. B. Stern, X. Ji, Y. Okawachi, A. L. Gaeta, and M. Lipson, "Battery-operated integrated frequency comb generator," Nature **562**, 401–405 (2018).
12. A. Hugi, G. Villares, S. Blaser, H. C. Liu, and J. Faist, "Mid-infrared frequency comb based on a quantum cascade laser," Nature **492**, 229–233 (2012).
13. T. Feng, L. Shterengas, T. Hosoda, A. Belyanin, and G. Kipshidze, "Passive mode-locking of 3.25 μm GaSb-based cascade diode lasers," ACS Photon. **5**, 4978–4985 (2018).
14. R. Q. Yang and S. S. Pei, "Novel type-II quantum cascade lasers," J. Appl. Phys. **79**, 8197–8203 (1996).
15. I. Vurgaftman, R. Weih, M. Kamp, J. R. Meyer, C. L. Canedy, C. S. Kim, M. Kim, W. W. Bewley, C. D. Merritt, J. Abell, and S. Höfling, "Interband cascade lasers," J. Phys. D **48**, 123001 (2015).
16. I. Vurgaftman, W. Bewley, C. Canedy, C. Kim, M. Kim, C. Merritt, J. Abell, J. Lindle, and J. Meyer, "Rebalancing of internally generated carriers for mid-infrared interband cascade lasers with very low power consumption," Nat. Commun. **2**, 585 (2011).
17. M. Kim, W. W. Bewley, C. L. Canedy, C. S. Kim, C. D. Merritt, J. Abell, I. Vurgaftman, and J. R. Meyer, "High-power continuous-wave interband cascade lasers with 10 active stages," Opt. Express **23**, 9664–9672 (2015).
18. J. L. Bradshaw, R. Q. Yang, J. D. Bruno, J. T. Pham, and D. E. Wortman, "High-efficiency interband cascade lasers with peak power exceeding 4 w/facet," Appl. Phys. Lett. **75**, 2362–2364 (1999).
19. C. L. Canedy, C. S. Kim, C. D. Merritt, W. W. Bewley, I. Vurgaftman, J. R. Meyer, and M. Kim, "Interband cascade lasers with > 40% continuous-wave wallplug efficiency at cryogenic temperatures," Appl. Phys. Lett. **107**, 121102 (2015).
20. L. A. Sterczewski, J. Westberg, C. L. Patrick, C. S. Kim, M. Kim, C. L. Canedy, W. W. Bewley, C. D. Merritt, I. Vurgaftman, J. R. Meyer, and G. Wysocki, "Multiheterodyne spectroscopy using interband cascade lasers," Opt. Eng. **57**, 011014 (2017).
21. M. Bagheri, C. Frez, L. A. Sterczewski, I. Gruidin, M. Fradet, I. Vurgaftman, C. L. Canedy, W. W. Bewley, C. D. Merritt, C. S. Kim, M. Kim, and J. R. Meyer, "Passively mode-locked interband cascade optical frequency combs," Sci. Rep. **8**, 3322 (2018).
22. H. Liu, G. Jenkins, E. Brown, K. McIntosh, K. Nichols, and M. Manfra, "Optical heterodyne detection and microwave rectification up to 26 GHz using quantum well infrared photodetectors," IEEE Electron Device Lett. **16**, 253–255 (1995).
23. J. Hillbrand, A. M. Andrews, H. Detz, G. Strasser, and B. Schwarz, "Coherent injection locking of quantum cascade laser frequency combs," Nat. Photonics **13**, 101–104 (2018).
24. Y. Yang, D. Burghoff, J. Reno, and Q. Hu, "Achieving comb formation over the entire lasing range of quantum cascade lasers," Opt. Lett. **42**, 3888–3891 (2017).
25. G. P. Agrawal, "Population pulsations and nondegenerate four-wave mixing in semiconductor lasers and amplifiers," J. Opt. Soc. Am. B **5**, 147–159 (1988).
26. D. Burghoff, T.-Y. Kao, N. Han, C. W. I. Chan, X. Cai, Y. Yang, D. J. Hayton, J.-R. Gao, J. L. Reno, and Q. Hu, "Terahertz laser frequency combs," Nat. Photonics **8**, 462–467 (2014).
27. D. Burghoff, Y. Yang, D. J. Hayton, J.-R. Gao, J. L. Reno, and Q. Hu, "Evaluating the coherence and time-domain profile of quantum cascade laser frequency combs," Opt. Express **23**, 1190–1202 (2015).
28. M. Singleton, P. Jouy, M. Beck, and J. Faist, "Evidence of linear chirp in mid-infrared quantum cascade lasers," Optica **5**, 948–953 (2018).
29. N. Opačak and B. Schwarz, "Theory of frequency modulated combs in lasers with spatial hole burning, dispersion and Kerr," arXiv:1905.13635v2 (2019).

30. G. Villares, A. Hugi, S. Blaser, and J. Faist, "Dual-comb spectroscopy based on quantum-cascade-laser frequency combs," Nat. Commun. **5**, 5192 (2014).
31. M. Rösch, G. Scalari, G. Villares, L. Bosco, M. Beck, and J. Faist, "On-chip, self-detected terahertz dual-comb source," Appl. Phys. Lett. **108**, 171104 (2016).
32. B. Schwarz, P. Reininger, H. Detz, T. Zederbauer, A. M. Andrews, S. Kalchmair, W. Schrenk, O. Baumgartner, H. Kosina, and G. Strasser, "A bi-functional quantum cascade device for same-frequency lasing and detection," Appl. Phys. Lett. **101**, 191109 (2012).
33. B. Schwarz, P. Reininger, D. Ristanić, H. Detz, A. M. Andrews, W. Schrenk, and G. Strasser, "Monolithically integrated mid-infrared lab-on-a-chip using plasmonics and quantum cascade structures," Nat. Commun. **5**, 4085 (2014).
34. B. Schwarz, C. A. Wang, L. Missaggia, T. S. Mansuripur, P. Chevalier, M. K. Connors, D. McNulty, J. Cederberg, G. Strasser, and F. Capasso, "Watt-level continuous-wave emission from a bifunctional quantum cascade laser/detector," ACS Photon. **4**, 1225–1231 (2017).
35. H. Lotfi, L. Li, S. M. S. Rassel, R. Q. Yang, C. J. Corrége, M. B. Johnson, P. R. Larson, and J. A. Gupta, "Monolithically integrated mid-IR interband cascade laser and photodetector operating at room temperature," Appl. Phys. Lett. **109**, 151111 (2016).
36. H. Lotfi, L. Li, L. Lei, H. Ye, S. M. S. Rassel, Y. Jiang, R. Q. Yang, T. D. Mishima, M. B. Santos, J. A. Gupta, and M. B. Johnson, "High-frequency operation of a mid-infrared interband cascade system at room temperature," Appl. Phys. Lett. **108**, 201101 (2016).
37. P. D. Grant, R. Dudek, M. Buchanan, and H. C. Liu, "Room-temperature heterodyne detection up to 110 GHz with a quantum-well infrared photodetector," IEEE Photon. Technol. Lett. **18**, 2218–2220 (2006).
38. B. Schwarz, P. Reininger, A. Harrer, D. MacFarland, H. Detz, A. M. Andrews, W. Schrenk, and G. Strasser, "The limit of quantum cascade detectors: a single period device," Appl. Phys. Lett. **111**, 061107 (2017).
39. M. Piccardo, D. Kazakov, N. A. Rubin, P. Chevalier, Y. Wang, F. Xie, K. Lascola, A. Belyanin, and F. Capasso, "Time-dependent population inversion gratings in laser frequency combs," Optica **5**, 475–478 (2018).